Geochemistry Geophysics Geosystems G3
AN ELECTRONIC JOURNAL OF THE EARTH SCIENCES
Published by AGU and the Geochemical Society

Article
Volume 7, Number 5
23 May 2006
Q05017, doi:10.1029/2005GC001045
ISSN: 1525-2027

Global compilation of variations in slab depth beneath arc volcanoes and implications

Ellen M. Syracuse and Geoffrey A. Abers

Department of Earth Sciences, Boston University, 685 Commonwealth Avenue, Room 131, Boston, Massachusetts, 02215, USA (syracuse@bu.edu)

[1] The location and motion of subducting plates relative to volcanic arcs provide a first-order constraint on theories of arc magmagenesis. We compile volcano-specific subduction parameters for 33,000 km of the global arc system at 839 volcanic centers, measuring the depth to the top of the slab (*H*) beneath each volcano. The compilation also includes estimates of slab strike and dip, incoming plate velocity, and age, all available in accompanying auxiliary material. The slab geometry is contoured from the top surface of Wadati-Benioff zones (WBZs) for a variety of teleseismic and local seismicity catalogs, which provides a reference surface for evaluating the distribution of seismicity within subducting plates. The WBZ thickness exceeds that expected from hypocentral errors in a manner correlating with plate age, indicating that old plates have thicker regions in which earthquakes can occur. When averaged over 500-km-long arc segments, *H* ranges from 72 to 173 km with a global average of 105 km, increasing by 20 km when hypocentral error effects are taken into account. These depths correlate poorly with most subduction parameters, but significant correlations exist between *H* and slab dip (correlation coefficient is 0.54 for 45 arc segments). The dip correlation can be explained if the melting region is displaced from the Wadati-Benioff zone by a constant-thickness boundary layer. For the north Pacific, *H* varies inversely with descent rate; this trend may reflect the manner in which wedge thermal structure affects arc location. Over short distances some arc segments exhibit abrupt variations in arc location but not slab geometry, indicating that upper-plate tectonic processes also exert control on *H*. These along-strike trends in *H* also correlate with geochemical proxies for the degree of melting, at least in one test case. Thus slab geometry and kinematics provide an important control on the melting that produces arc volcanoes.

Components: 10,464 words, 14 figures, 1 table, 1 dataset.

Keywords: slab geometry; slab dip; Wadati-Benioff zone; slab thickness; descent rate.

Index Terms: 7240 Seismology: Subduction zones (1207, 1219, 1240); 7230 Seismology: Seismicity and tectonics (1207, 1217, 1240, 1242); 8185 Tectonophysics: Volcanic arcs.

Received 13 June 2005; **Revised** 6 February 2006; **Accepted** 15 March 2006; **Published** 23 May 2006.

Syracuse, E. M., and G. A. Abers (2006), Global compilation of variations in slab depth beneath arc volcanoes and implications, *Geochem. Geophys. Geosyst.*, *7*, Q05017, doi:10.1029/2005GC001045.

1. Introduction

[2] Volcanism occurs at the majority of subduction zones along arcs roughly parallel to the trench. It is often stated that the top of the slab below front arc volcanoes is at a depth of roughly 100–120 km (108 ± 14 km [*Tatsumi and Eggins*, 1995]; 112 ± 19 km [*Tatsumi*, 1986]; 124 ± 38 km [*Gill*, 1981]), and that this depth (*H*) is the same for all subduction zones, regardless of slab dip and plate age [*Davies and Stevenson*, 1992]. Typically, the slab top is defined as the top of the Wadati-Benioff zone (WBZ), often the clearest representation of the downgoing plate. Many high-resolution studies have shown that the upper surface of the WBZ lies within a few km of a discontinuity thought to represent the uppermost slab surface, at least at depths < 200 km [e.g., *Zhao et al.*, 1997; *Yuan et*

al., 2000; *Nakajima et al.*, 2001; *Ferris et al.*, 2003]. The constancy in *H* has led to the inference that a pressure-controlled process triggers magma generation, such as a dehydration reaction within or just above the slab [e.g., *Tatsumi*, 1986; *Davies and Stevenson*, 1992]. However, recent experiments [*Schmidt and Poli*, 1998; *Kerrick and Connolly*, 2001] indicate nearly continuous breakdown of hydrous phases in the slab, so melts could form above a slab at any depth where temperatures exceed the appropriate solidus. Thus an obvious dehydration "trigger" seems less viable than when first proposed, and wedge thermal structure may be more important in localizing arc volcanism.

[3] One approach to testing models of arc magmagenesis has been to seek correlations between potentially relevant subduction-related parameters such as slab age, convergence rate, and slab dip. By analyzing seismicity from the "EHB" earthquake catalog [*Engdahl et al.*, 1998], *England et al.* [2004] inferred that *H* varies from 65 km to 130 km in different arc segments in a manner that correlates with slab descent rate. They find that *H* is most greatly influenced by the slab dip and plate convergence velocities, and conclude that the temperature structure of the mantle wedge, rather than the dehydration of the slab, may control the site of volcanism [*England and Wilkins*, 2004].

[4] However, WBZ geometries reflect both processes within the slab and hypocentral errors. For example, while local seismicity data sets show that WBZs are composed of one or two planes of seismicity no more than a few km thick [e.g., *Abers*, 1992; *Igarashi et al.*, 2001], such observations are absent in most subduction zones, and global catalogs show WBZ thicknesses of several tens of km. Hence, even the first-order systematics of WBZ structure are not easily available, and it remains unclear (for example) whether *H* is biased by hypocentral error, or whether double seismic zones are abundant or rare.

[5] Arc geochemistry provides another indicator of the causes of melting. *Plank and Langmuir* [1988] show a global correlation between geochemical proxies for degree of melting and the upper-plate crustal thickness, interpreted as a proxy for the top of the mantle-melting column. Their analysis assumes constant *H*, but it seems likely that if *H* varies by a factor of two among arcs, then the extent of melting should vary accordingly.

[6] To evaluate these issues, we have created a global catalog of slab-related parameters for 839 volcanoes in 51 sections of arc (Figure 1). The primary new contribution is a separate estimate of *H* for each volcano and averages for 500-km arc segments, presented in the auxiliary material[1] as a digital resource, and analysis of that database. The database also includes updated estimates of several basic plate parameters (convergence velocity, incoming plate age, slab dip, etc.) tabulated on a per-volcano basis. The remainder of this paper describes the methodology used, analyzes uncertainties, and presents some first-order analyses. Variations of a factor of 2–3 in *H* exist, including regional variations up to 80 km within individual arc segments. These regional variations demonstrate importance of factors other than the temperature structure of the mantle wedge in localizing arc volcanism. Finally, we observe that the width of the WBZ varies globally with slab age, and in one test case, *H* varies along strike with chemical indicators of the degree of melting.

2. Methods

2.1. Determining Slab Depth

[7] Contours of the top of the Wadati-Benioff zone (WBZ) (auxiliary material Table S3) are based on hypocenters from the EHB earthquake catalog (version 64-02) [*Engdahl et al.*, 1998]. In order to ensure depth accuracy we consider only earthquakes with formal depth errors <15 km, formal horizontal errors <35 km, and located with three or more depth phases (*pP*, *pwP* or *sP*). This is the strictest depth-phase criterion for which sufficient earthquakes exist to contour the WBZ for all arcs. The scatter in earthquake positions relative to the digitized WBZ surface is similar with stricter depth-phase criteria, but fewer events can be contoured. Formal errors show large regional variations so it is difficult to use them for more stringent quality control (section 3.3).

[8] The top of the WBZ serves as a proxy for the top of the downgoing plate, following previous studies that find the two generally coincide to within a few km [e.g., *Nakajima et al.*, 2001; *Zhao et al.*, 1997; *Yuan et al.*, 2000]. For each subduction zone (Figure 1), cross sections of the seismicity are made parallel to the local direction of maximum WBZ dip at along-strike intervals of $\leq 1^\circ$, projecting hypocenters within 50 km of the section line and ignoring hypocenters with depths <30 km. The top of the WBZ is visually estimated at depth intervals of 50 km, such that the resulting surface lies above approximately 95% of all hypo-

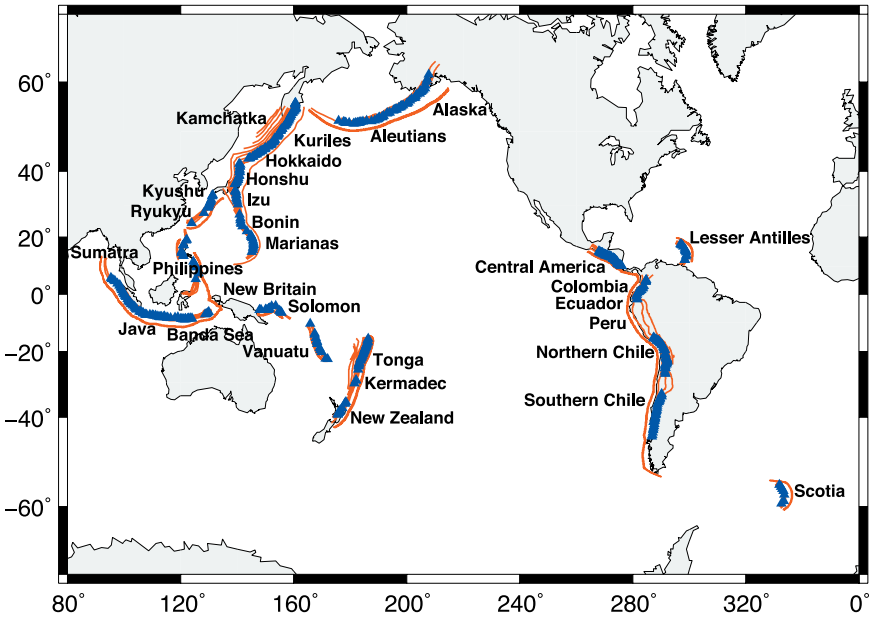

Figure 1. Map of the arc sections discussed in this paper, with slab contours (curves) and volcanoes (triangles).

centers at depths 55–250 km. For seismicity gaps of less than 100 km depth, the contours are linearly interpolated. By comparison, *England et al.* [2004] project both seismicity and volcanoes for several hundred km along small circles, a procedure that assumes both an uncontorted slab and the same axis of curvature for slab and arc, within each segment. At the trench and seaward, we equate the top of the downgoing plate with the seafloor, here approximated as a 6 km isobath at the trench, a global average. A surface is fitted to these seafloor and WBZ contours and then interpolated with the method of *Wessel and Smith* [1991]; this surface is referred to as the "slab surface." By concentrating on the details of the upper 250 km of seismic zones, this procedure provides a slab surface that much more closely resembles subarc seismicity than a previous global compilation devised for parameterizing global tomography [*Gudmundsson and Sambridge*, 1998]; see comparison in Figure 2.

[9] The Cascadia, Mexican and Mediterranean subduction zones are excluded for insufficient seismicity. The Molucca Sea – Sulawesi region is excluded for its complexity. In the northern Andes, WBZ seismicity ceases trenchward of the volcanic front so H cannot be determined, but other parameters are tabulated. For points east of 86°W in Central America, hypocenters from *Protti et al.* [1994] are used to model sharp contortions.

[10] Most volcano locations come from the Smithsonian catalog [*Siebert and Simkin*, 2002], including only those thought to have erupted during the Holocene. In Central America, we use the volcano catalog of *Carr et al.* [2003]. Additional submarine volcanoes in Tonga and Kermadec are also included from *Arculus* [2003, 2004]. The depth of the slab surface beneath each volcano, H, is interpolated from the digitized surface, wherever it could be estimated beneath volcanoes.

[11] The parameter H is also averaged, from arc-front volcanoes, in 500 km long arc segments worldwide, to provide uniform sampling. A volcano is defined to be at the arc front if it is closer than its immediate neighbor volcanoes, within a few tens of km along strike. Figure 3 shows H and other parameters for one arc system, as an example.

2.2. Determining Dip, Convergence Velocity, and Slab Age

[12] From the digitized surfaces, slab dip (δ) is averaged in the direction of maximum dip, between 50 km and 250 km depth. This procedure removes a natural correlation between δ and H on a steepening slab. The dip direction is not necessarily perpendicular to the trench, nor always parallel to the direction of convergence. The minimum depth limit of 50 km coincides with the downdip limit of typical thrust zones [*Tichelaar and Ruff*, 1993]. In areas where the WBZ does not extend to 250 km depth, δ is averaged from the 50 km depth to the deepest earthquakes. For each volcano, the strike of the slab is defined as that perpendicular to the

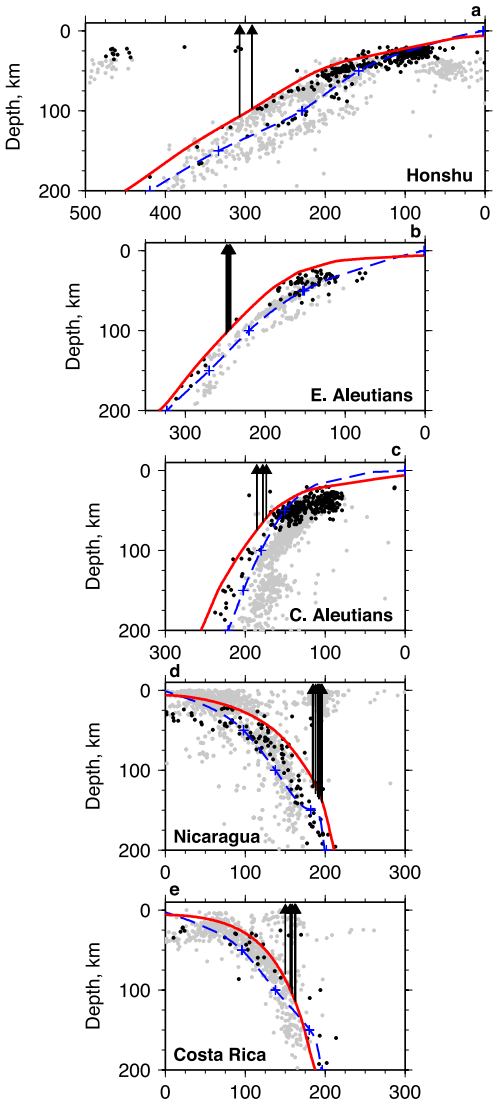

Figure 2. Comparisons of the EHB catalog (dark circles) and local catalogs (light circles). Teleseismic events projected 100 km from cross section, and local events projected 50 km. The solid red curve represents the slab surface based on the EHB seismicity. As a comparison, the dashed blue curve represents a surface fitted to the contours (blue crosses) from *Gudmundsson and Sambridge* [1998]. (a) The JUNEC catalog [*Tsuboi*, 1992] indicates a slab surface approximately 5 km shallower. Cross-section location shown in Figure 3d. (b) The Eastern Aleutian Seismic Network earthquakes [*Abers*, 1992] indicate a slab surface approximately 10–15 km deeper. Cross-section location shown in auxiliary material Figure S3d. (c) Central Aleutian earthquakes [*Kisslinger*, 1993] indicate a slab surface approximately 25 km deeper. Cross-section location shown in auxiliary material Figure S3d. (d) Nicaragua local catalog [*Strauch et al.*, 2004] and (e) Costa Rica local catalog [*Protti et al.*, 1994] indicate a slab surface up to 75 km deeper in Nicaragua and an uncertain difference in Costa Rica. Cross-section locations shown in auxiliary material Figure S2d.

direction of maximum dip as measured from the underlying slab surface. At slab tears or sharp contortions, the strike of the trench is used. For volcanoes without underlying seismicity, slab strike is based on that of neighboring volcanoes.

[13] Where possible convergence velocities are estimated from magnetic lineations [*DeMets et al.*, 1994], which average over timescales comparable to plate descent times, but for many arcs the upper-plate velocities cannot be well determined from magnetic lineations and GPS-based velocities are used. All sources for convergence velocities and plate ages are listed in auxiliary material Table S1 [*DeMets et al.*, 1994; *Gorbatov and Kostoglodov*, 1997; *Kato et al.*, 2003; *Muller et al.*, 1997; *Sella et al.*, 2002; *Taylor et al.*, 1995; *Thomas et al.*, 2003; *Wallace et al.*, 2004; *Zellmer and Taylor*, 2001]. Plate velocities at the Lesser Antilles are calculated by using the Caribbean – North American plate pair, since the boundary between the North and South American plates is not well known, and the Caribbean - South American velocity is only 0.6 km/Ma slower. Plate velocities for the Ryukyu arc are calculated by using the Philippine – South China plate pair, although it is somewhat unclear as to whether the South China or the Amurian plate should be considered to be the upper plate. If the Amurian plate is used, convergence velocities decrease on average by 4 km/Ma. For arcs with back-arc spreading or compression, we calculated both convergence velocities with (auxiliary material Tables S1b and S2b)[1] and without (Table 1; auxiliary material Tables S1a and S2a) upper plate strains taken into account. All plate velocities are also corrected for obliquity such that "V_c" in the tables represents the arc-normal component.

[14] The seafloor age at the trench is determined as the age of material entering the trench along a flowline to each volcano, by backtracking along convergence directions. Where available, the age comes from the compilation from *Müller et al.* [1997]; otherwise the age comes from *Gorbatov and Kostoglodov* [1997] if available. Ages for the seafloor near Java between 105° and 114° longitude are interpolated between seafloor ages to the east and west of this segment. Incoming plate ages were not available for the New Britain and Solomon arcs, much of Ryukyu, and Banda east of 121° longitude, near where Australian continental crust is subducting [*Bowin et al.*, 1980]. In many places

[1] Auxiliary material is available at ftp://ftp.agu.org/apend/gc/2005gc001045.

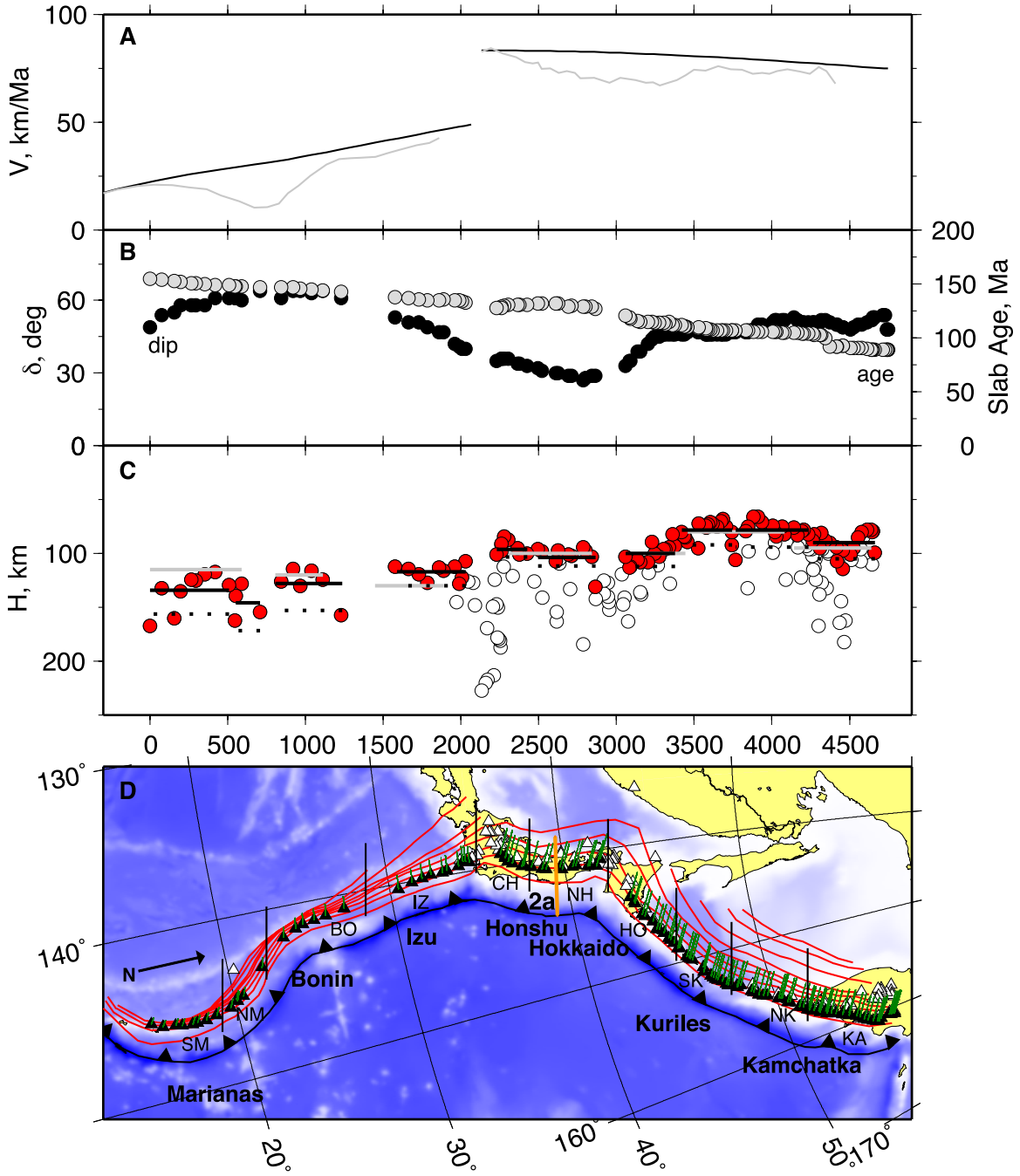

Figure 3. Kamchatka through Marianas. (a) Convergence velocity. Black line indicates relative plate velocity, gray line indicates plate velocity corrected for obliquity and smoothed; both do not consider back-arc spreading rates. (b) δ for front-most volcanoes in black, age of incoming plate at trench for front-most volcanoes in gray. (c) *H* for front-most volcanoes (red) and for further back volcanoes (white). Black lines indicate average H of front-most volcanoes for 500-km arc sections; dotted lines indicate *H′*; gray lines indicate *H* calculated by *England et al.* [2004]. (d) Black triangles represent front-most volcanoes, white triangles represent other volcanoes, red lines indicate slab contours at 50-km intervals for depths less than 300 km and 100-km intervals for depths greater than 300 km, green lines indicate direction and relative magnitude of convergence, and black lines give approximate locations of boundaries between 500-km arc sections, labeled with their abbreviations. Orange lines indicate the locations of cross sections shown in other figures. For additional arcs, see auxiliary material Figures S1–S12.

seafloor created during the Cretaceous Quiet Zone is entering the trench, so uncertainties can exceed 10–20 Ma.

[15] We also tabulate two derived parameters previously proposed to scale with subduction-zone thermal structure. The slab descent rate, $V_c \sin \delta$, should drive the rate of flow in the mantle wedge [*England et al.*, 2004]. The "thermal parameter" Φ, the product of plate age and descent rate, should scale to the maximum depth of a given isotherm within the subducting plate [e.g., *Kirby et al.*, 1996].

3. Robustness and Uncertainty

[16] Uncertainties in all parameters are calculated for each arc segment as the 2-σ standard deviation of the mean for measurements from individual volcanoes (Table 1). Systematic errors may also exist for a variety of reasons: the slab surface may be incorrectly digitized, hypocenters may be systematically mislocated due to long-wavelength earth structure, hypocenters may be randomly mislocated thereby widening the WBZ, or along-strike averaging may distort local variations in H. We test below several of these effects, and find that hypocentral location errors can produce large but correctable systematic biases.

3.1. Comparisons With Local Catalogs

[17] At well-monitored subduction zones local catalogs provide an independent test of the slab surfaces. At depths exceeding network aperture the hypocenters can be biased toward the trench, due to the fast travel times in a high-velocity slab [*McLaren and Frolich*, 1985; *van der Hilst and Engdahl*, 1992]. For similar reasons, local catalogs can be more accurate than teleseismic catalogs for events shallower than 200 km if the network geometry is favorable. In central Japan, the Japan University Network Earthquake Catalog [*Tsuboi*, 1992] shows H to be within five km of that indicated by the EHB catalog (Figure 2a). Data from the Eastern Aleutian Seismic Network [*Abers*, 1992] suggest that H is 10–15 km deeper than determined here (Figure 2b). In the central Aleutians, the Adak network data [*Kisslinger*, 1993] indicate that H is 25 km deeper and the slab dips more steeply than measured here (Figure 2c), but problems with earthquake depth caused by a narrow network geometry have been previously identified in this catalog [*Kisslinger*, 1993]. In Nicaragua (Figures 2d and 2e), the near-vertically dipping WBZ inferred from local data indicates a slab up to 75 km deeper than ours [*Protti et al.*, 1994; *Strauch et al.*, 2004], but network coverage is poor there. In adjacent Costa Rica large scatter in the small number of EHB earthquakes makes it difficult to infer values of H from teleseismic locations, but the local catalog defines it clearly.

[18] For the clearest of these comparisons, where local catalogs seem robust (Japan, East Aleutians, Costa Rica), the local catalog shows H within 5–15 km compared with EHB, comparable with uncertainty estimates.

3.2. Variability of Digitization and Repeatability

[19] To assess errors in the manual surface digitization process, two other seismologists (L. Auger and G. Rossi) repeated the process for the Aleutians. An average maximum difference in H of 10 km was found between the three digitized surfaces, preserving relative variations in H (Figure 4). The errors due to the digitization process should contribute a maximum of 10 km of error in H.

3.3. Hypocenter Errors

[20] Any errors in hypocenters will act to increase the apparent thickness of the WBZ. Because the slab surface represents the top of the WBZ, not its center, H will be biased toward small values, since random hypocentral error acts to increase WBZ width. Here, we evaluate the extent of this potential bias, and devise an approximate correction.

[21] To estimate the thickness of the WBZ, the closest distance from the digitized surface is calculated for each earthquake between 55 km and 250 km depth. For each 500-km section of arc, we calculate the statistical distribution of this slab-normal distance of hypocenters away from the slab surface (e.g., Figure 5). Within each 500-km section of arc, 90–100% of all earthquakes lie beneath the WBZ surface, for all arc sections (auxiliary material Table S1). Thus the WBZ surfaces appear to be digitized consistently near or at the top of seismicity.

[22] As a pessimistic estimate of earthquake mislocation, we could assume that that all hypocenters actually lie on a single surface parallel to that digitized and that all scatter represents hypocenter error. In this case, the true seismicity surface would go through the middle of the distribution of earthquakes, not at its top where digitized. Because the vertical distribution of earthquakes is on average

Table 1. Average Parameters for 500-km Sections of Arc

Arc Name	Short Name	H, km	H′, km	δ, deg	Vtot, km/Ma	Vc, km/Ma	Age, Ma	Descent Rate, km/Ma	Φ/100, km	WBZ Thickness, km	ef
Colombia	CO	-	-	32.7 ± 1.9	66.7 ± 0.7	54.9 ± 2.3	13.3 ± 1.3	29.3 ± 0.7	3.9 ± 0.4	40.4	4.0
Ecuador	EC	-	-	19.3 ± 4.7	69.4 ± 0.4	67.0 ± 0.4	18.0 ± 1.2	22.2 ± 4.8	4.0 ± 0.6	49.2	5.6
North Peru Gap	NPG	-	-	10.0 ± 0.4	72.9 ± 0.7	69.5 ± 3.1	29.0 ± 0.4	12.0 ± 0.7	3.5 ± 0.5	48	6.3
Central Peru Gap	CPG	-	-	11.7 ± 1.0	75.6 ± 0.7	66.7 ± 2.8	33.9 ± 4.0	13.6 ± 1.7	4.7 ± 1.0	50.8	5.7
Peru	PE	99.6 ± 3.8	114.3	28.7 ± 1.0	78.4 ± 0.2	65.1 ± 3.2	42.1 ± 0.9	31.4 ± 4.4	13.4 ± 2.1	47.2	6.4
North Chile	NC	112.5 ± 5.6	127.5	29.3 ± 1.0	79.9 ± 0.1	79.0 ± 0.5	46.2 ± 0.6	38.7 ± 1.1	17.8 ± 0.7	32.4	6.6
North Central Chile	NCC	109.8 ± 7.1	123.0	23.6 ± 1.9	80.7 ± 0.4	77.4 ± 0.7	42.8 ± 0.6	30.9 ± 2.4	13.3 ± 1.2	34.4	6.0
Central Chile Gap	CCG	-	-	14.1 ± 1.9	81.1 ± 0.1	73.8 ± 2.2	37.7 ± 1.4	17.8 ± 1.8	6.7 ± 0.5	45.6	5.3
Central Chile	CC	102.9 ± 6.1	114.4	27.5 ± 0.8	81.0 ± 0.2	71.6 ± 1.5	32.4 ± 0.8	33.1 ± 1.4	10.7 ± 0.3	20.8	5.1
South Central Chile	SCC	80.1 ± 3.5	96.6	34.6 ± 0.0	80.4 ± 0.5	74.7 ± 1.3	23.5 ± 2.1	42.3 ± 1.8	9.8 ± 0.5	-	-
South Chile	SC	-	-	-	79.6 ± 0.5	74.9 ± 0.2	10.3 ± 3.6	-	-	-	-
Guatemala/El Salvador	GE	104.9 ± 7.2	131.6	56.9 ± 1.5	67.7 ± 1.1	66.9 ± 1.2	17.4 ± 0.3	55.9 ± 1.9	9.7 ± 0.5	32	7.3
Nicaragua	NI	132.9 ± 4.1	164.0	62.2 ± 0.6	75.5 ± 0.6	71.1 ± 0.9	17.5 ± 0.3	62.8 ± 0.7	11.0 ± 0.2	35.6	7.3
Costa Rica	CR	96.5 ± 8.0	122.4	58.9 ± 4.6	80.1 ± 0.7	75.4 ± 1.6	15.8 ± 0.2	63.9 ± 2.5	10.1 ± 0.5	65.2	6.7
Alaska	AK	84.9 ± 4.6	94.9	42.0 ± 1.8	57.4 ± 0.5	49.0 ± 2.9	47.1 ± 0.8	33.0 ± 2.9	15.6 ± 1.6	28	3.7
Alaska Peninsula	AP	92.1 ± 4.9	103.2	45.0 ± 1.3	60.8 ± 0.8	59.0 ± 1.9	52.2 ± 0.9	41.8 ± 2.1	22.0 ± 1.5	30	3.9
East Aleut	EA	85.4 ± 5.2	98.8	45.6 ± 1.2	64.7 ± 0.7	64.2 ± 0.8	55.3 ± 0.4	45.9 ± 1.4	25.4 ± 0.9	29.2	4.7
Central Aleut	CA	72.3 ± 8.6	90.4	53.7 ± 1.4	68.3 ± 0.7	63.4 ± 1.9	55.9 ± 0.4	51.0 ± 0.8	28.4 ± 0.5	31.6	5.4
West Aleut	WA	78.4 ± 8.0	98.5	55.9 ± 2.4	71.5 ± 0.4	50.2 ± 7.4	56.1 ± 0.5	42.0 ± 6.7	23.5 ± 3.7	29.2	5.6
Kamchatka	KA	90.1 ± 4.8	105.1	50.7 ± 0.8	76.3 ± 0.3	75.1 ± 0.7	92.9 ± 2.2	58.2 ± 0.8	54.1 ± 1.8	35.2	4.8
North Kurile	NK	78.5 ± 4.6	94.2	50.4 ± 1.0	78.8 ± 0.3	78.3 ± 0.3	105.6 ± 0.5	60.2 ± 0.7	63.6 ± 0.5	45.6	5.0
South Kurile	SK	78.3 ± 3.9	92.0	46.4 ± 0.2	80.5 ± 0.2	77.4 ± 1.3	108.5 ± 0.8	56.0 ± 0.9	60.7 ± 0.6	45.2	4.7
Hokkaido	HK	100.2 ± 4.8	112.1	41.9 ± 2.6	81.8 ± 0.6	74.7 ± 0.6	115.2 ± 1.4	49.7 ± 2.2	57.2 ± 2.0	42.8	4.4
North Honshu	NH	103.6 ± 9.5	111.5	28.7 ± 0.7	82.9 ± 0.2	81.6 ± 0.9	129.3 ± 1.1	39.2 ± 0.7	50.7 ± 1.1	36	3.5
Central Honshu	CH	96.2 ± 4.0	103.3	33.9 ± 1.3	83.3 ± 0.2	82.7 ± 0.5	130.5 ± 0.9	46.3 ± 1.7	60.4 ± 2.0	48	3.0
Izu	IZ	117.0 ± 4.4	130.2	46.1 ± 3.1	46.3 ± 1.4	45.6 ± 1.7	135.4 ± 0.9	32.6 ± 0.8	44.1 ± 1.3	42.4	4.6
Bonin	BO	127.8 ± 12.7	152.9	62.8 ± 1.2	34.5 ± 1.6	31.6 ± 4.3	145.3 ± 1.3	28.1 ± 3.9	40.8 ± 5.4	53.6	5.7
North Marianas	NM	145.8 ± 15.2	171.5	61.5 ± 1.7	28.8 ± 0.9	15.3 ± 1.3	147.8 ± 0.5	13.4 ± 0.9	19.9 ± 1.4	41.6	6.1
South Marianas	SM	134.2 ± 11.8	156.2	56.9 ± 2.5	24.5 ± 1.4	20.5 ± 0.4	151.6 ± 1.4	17.1 ± 0.6	25.9 ± 0.7	48	6.0
Kyushu	KY	104.8 ± 11.6	120.0	53.8 ± 2.8	73.8 ± 1.5	72.0 ± 2.6	27.0 ± 1.7	57.6 ± 0.6	15.6 ± 1.0	26.8	4.5
Ryukyu	RY	71.5 ± 23.0	83.3	43.5 ± 3.0	84.2 ± 7.7	69.5 ± 20.2	43.0 ± 0.0	48.1 ± 16.4	17.1 ± 0.0	26.4	4.3
North Philippines	NP	120.8 ± 15.0	139.8	57.4 ± 3.5	100.9 ± 1.3	87.7 ± 8.2	32.4 ± 2.3	73.1 ± 5.0	23.6 ± 3.2	31.6	5.1
South Philippines	SP	162.2 ± 25.7	191.4	64.3 ± 7.6	105.0 ± 1.4	69.0 ± 9.8	59.8 ± 0.4	62.0 ± 11.3	36.3 ± 8.1	47.6	6.3
New Britain	NB	126.6 ± 35.8	159.6	68.2 ± 3.0	82.1 ± 1.7	29.7 ± 6.5	-	27.4 ± 6.0	-	45.6	6.1
Solomon	SO	154.0 ± 20.2	191.0	70.4 ± 5.3	96.8 ± 4.9	93.0 ± 8.6	-	87.5 ± 10.7	-	40.8	6.2
North Vanuatu	NV	188.0 ± 16.3	208.0	71.3 ± 5.7	89.1 ± 3.5	74.4 ± 25.9	44.0 ± 16.2	69.7 ± 22.5	32.5 ± 19.4	32	5.6
South Vanuatu	SV	101.8 ± 40.2	147.6	66.8 ± 1.3	76.1 ± 2.6	57.3 ± 21.3	50.0 ± 0.0	52.5 ± 19.1	26.2 ± 9.5	30	6.1
Tonga	TO	88.1 ± 5.9	110.4	52.4 ± 0.7	77.3 ± 1.4	73.3 ± 2.4	109.0 ± 0.0	58.1 ± 2.1	63.3 ± 2.2	56	6.8
Kermadec	KE	91.4 ± 8.6	121.1	56.1 ± 2.8	66.3 ± 3.0	64.6 ± 3.7	105.6 ± 2.8	53.5 ± 2.4	56.6 ± 3.9	48.4	8.3
New Zealand	NZ	123.4 ± 19.6	146.8	52.0 ± 2.0	45.5 ± 1.5	30.4 ± 5.7	100.0 ± 0.0	24.2 ± 5.1	24.2 ± 5.1	56	7.2
North Sumatra	NS	119.3 ± 11.1	138.3	49.1 ± 1.6	51.7 ± 1.2	41.5 ± 2.1	48.3 ± 1.9	31.2 ± 1.3	15.1 ± 0.6	56.4	6.2
Central Sumatra	CS	100.6 ± 9.1	118.3	46.4 ± 0.8	55.5 ± 0.7	40.0 ± 1.8	54.8 ± 3.9	29.0 ± 1.6	15.9 ± 1.7	36.4	6.1
South Sumatra	SS	88.7 ± 9.8	108.0	50.2 ± 0.5	59.1 ± 0.7	48.7 ± 2.5	68.9 ± 2.4	37.4 ± 1.7	25.9 ± 2.1	49.6	6.5
Sunda Strait	ST	90.3 ± 6.8	109.3	49.3 ± 0.5	63.6 ± 0.8	61.0 ± 1.6	85.5 ± 3.9	46.3 ± 1.2	39.6 ± 2.6	61.2	6.2
Java	JV	151.9 ± 11.1	172.4	45.8 ± 1.2	68.2 ± 0.8	67.8 ± 1.0	111.2 ± 5.2	48.6 ± 0.6	54.0 ± 2.5	57.2	7.2
Bali/Lombok	BL	167.4 ± 12.9	186.8	45.9 ± 3.2	71.1 ± 0.7	69.8 ± 0.4	134.9 ± 4.5	50.1 ± 2.4	67.7 ± 5.3	74	7.3
West Banda Sea	WB	115.0 ± 6.9	119.6	54.4 ± 2.2	76.1 ± 0.3	73.6 ± 0.5	-	59.8 ± 1.3	-	48.8	6.1
East Banda Sea	EB	141.8 ± 22.0	160.5	48.0 ± 4.3	78.8 ± 0.4	25.3 ± 19.1	-	19.5 ± 15.0	-	55.6	6.3
North Lesser Antilles	NA	107.8 ± 5.1	120.5	49.8 ± 0.4	19.3 ± 0.2	17.6 ± 0.8	83.0 ± 0.8	13.4 ± 0.6	11.1 ± 0.5	33.2	4.1
South Lesser Antilles	SA	121.8 ± 4.7	136.2	42.4 ± 3.9	19.6 ± 0.1	17.9 ± 0.9	86.6 ± 1.7	12.1 ± 1.5	10.4 ± 1.1	35.2	5.3
Scotia	SCO	95.7 ± 21.2	133.6	64.6 ± 3.4	7.3 ± 0.1	6.0 ± 1.4	59.1 ± 15.3	5.4 ± 1.3	3.5 ± 1.3	42.4	8.1

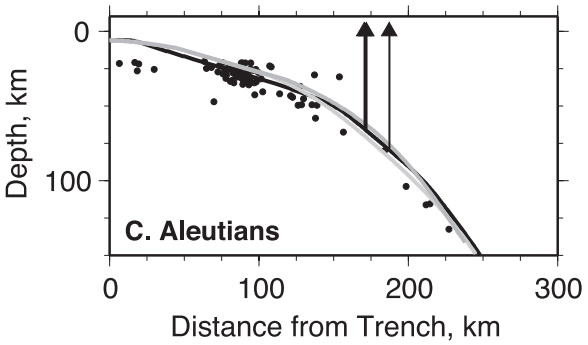

Figure 4. Comparison of the digitized slab (black line) with those made by two other seismologists (gray lines) through the Eastern Aleutians. Circles: EHB catalog hypocenters. Cross-section location shown in auxiliary material Figure S3d.

60 km wide, after correcting for dip, this error model would imply that H is biased by 30 km toward small values (see section 4.1). This extreme correction does not change any of the correlations between H and other parameters discussed in section 4.

[23] Alternatively, the formal errors from earthquake locations calculated by *Engdahl et al.* [1998] may provide a good description of hypocentral errors, and scatter in excess of them may reflect real WBZ structure. Commonly, formal errors underestimate true hypocentral errors [e.g., *Pavlis*, 1986], but it is possible that the EHB error estimation method is complete. To test this proposition, the apparent thickness of the WBZ within each slab segment is estimated as four times the standard deviation of the distance of hypocenters to the slab surface (Figure 6, Table 1). We consider only segments with >10 EHB earthquakes meeting selection criteria. This WBZ thickness is compared with formal errors in the EHB catalog, here taken as the Pythagorean average of vertical and horizontal reported uncertainties, averaged for each arc segment as e_f. The e_f vary by a factor of 3 from region to region (Figure 6), reflecting variations in global monitoring. The apparent WBZ thickness exceeds $4e_f$ by 0.4–45 km, or 19 km on average. At least some of the apparent WBZ thicknesses come close to that predicted from formal errors so it seems likely that the formal errors do not grossly underestimate actual uncertainties; taken at face value the hypocentral uncertainties explain roughly half the WBZ thickness. Also, correlations exist between apparent WBZ thickness and plate age (section 4.4), an observation that seems difficult to explain were the apparent WBZ thickness entirely due to hypocentral mislocation. Hence e_f represents a useful minimum estimate of the effect of hypocentral mislocation on H, and perhaps an accurate estimate.

[24] To correct for the bias due to hypocentral errors, we adjust the slab depth to H' where

$$H' = H + 2e_f / \cos\delta$$

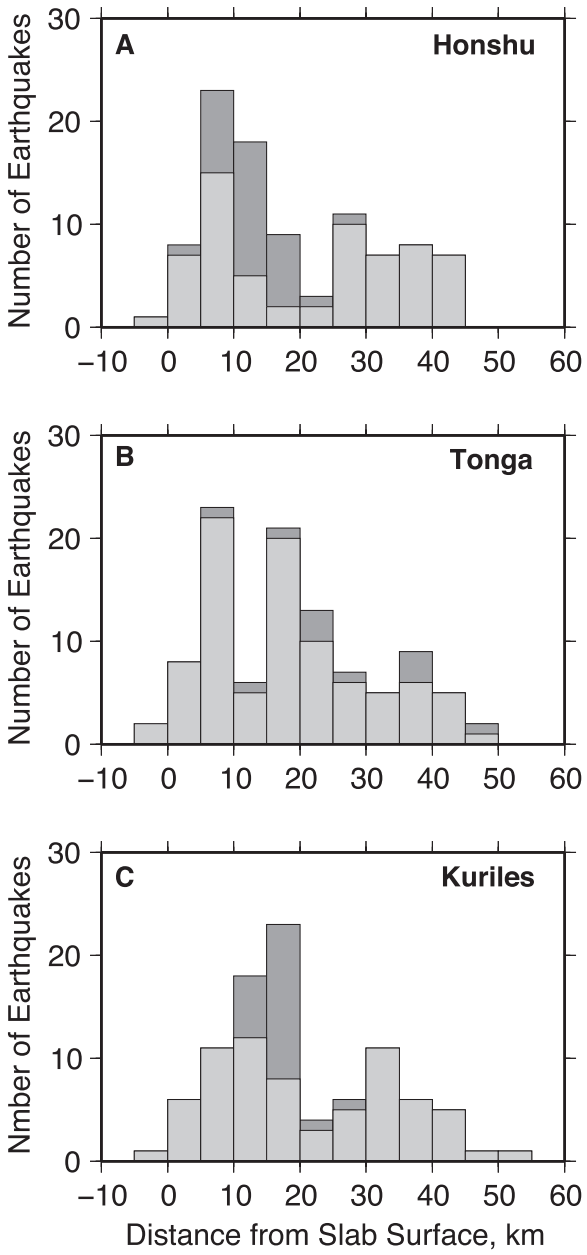

Figure 5. Histograms for distance of earthquakes from inferred slab surfaces at intermediate depths beneath (a) Honshu, (b) Tonga, and (c) the Kuriles, where double seismic zones have been suggested previously. Dark histograms represent earthquakes with depths between 55 and 250 km; light histograms represent depths between 70 and 250 km. Note bimodal distribution most obvious in Honshu.

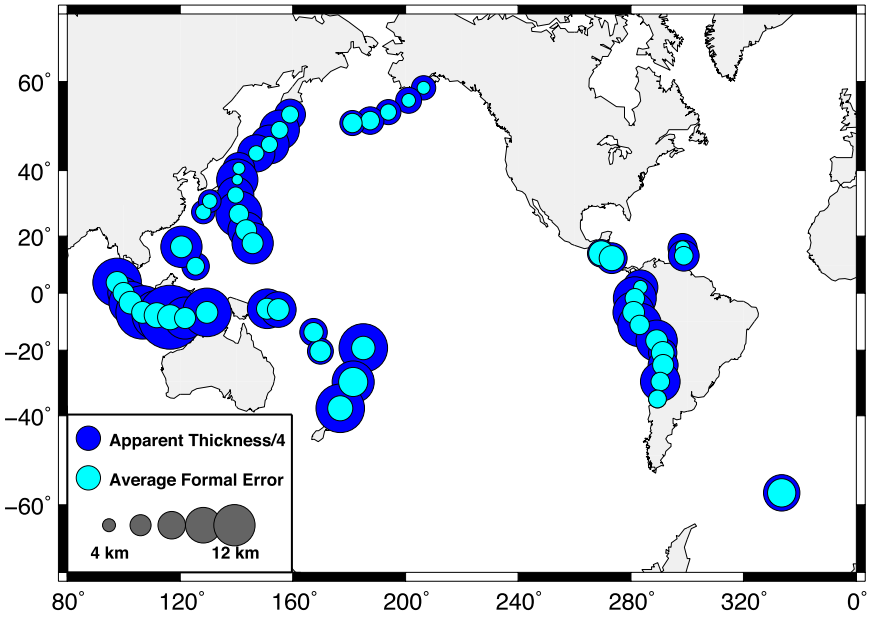

Figure 6. Map comparing apparent width of slabs to reported formal errors of earthquake locations for each parameter averaged over 500-km sections of arc that contain more than 10 earthquakes from the EHB catalog.

since the e_f represent a 1-sigma uncertainty estimate. All correlations of arc segments use H', but because e_f represents an average for each arc segment we present uncorrected H when discussing individual volcanoes.

3.4. Comparison With Results From *England et al.* [2004]

[25] *England et al.* [2004] also used the EHB catalogs to determine average arc-slab depth for many of the same arc segments. The H calculated in this study tend to be shallower than those from *England et al*. by an average of 2 km and correlate closely (Figure 7), such that almost all lie within 15 km between the two studies. We compare H rather than H' because *England et al.* [2004] did not correct for hypocenter error. Overall, the consistency suggests that the large variations in H between arc segments are a robust feature of the EHB data set. Java shows the largest discrepancy, where a sharp jump in H within western Java was not noticed previously (section 4.3.1). If H varies systematically within an arc segment, *England et al.*'s [2004] procedure may result in estimates near the minimum of the range, because it takes the uppermost events to represent the slab surface after projecting the entire arc segment onto a single cross section. In the Marianas, our average H agrees better with that predicted from local data (D. Wiens, personal communication, 2005).

4. Results and Discussion

4.1. Global Ranges

[26] The compilation of parameters from all frontal arc volcanoes (Figure 3; auxiliary material Figures S1–S11; auxiliary material Table S2a

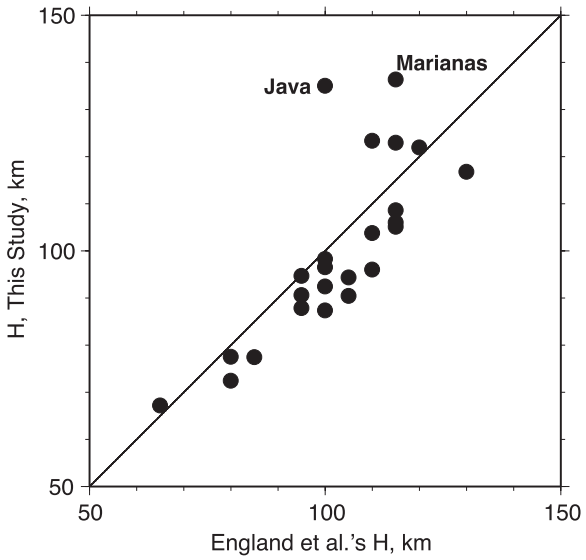

Figure 7. Comparison of H from *England et al.* [2004] with this study. We average volcanoes over the arc segments shown by *England et al.* [2004] for the same sets of volcanoes for comparison. Values from this study are routinely 2 km shallower.

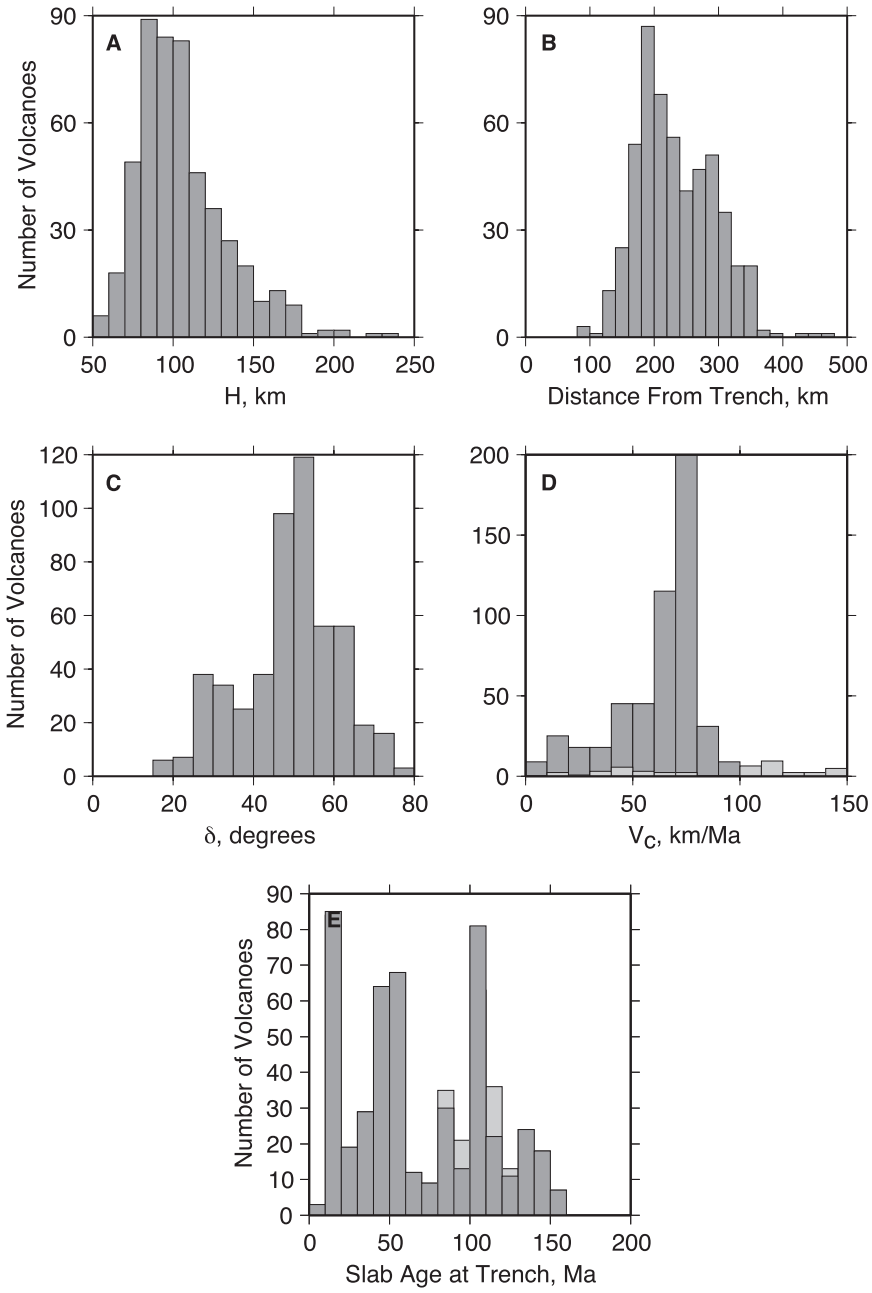

Figure 8. Histograms of H, distance from trench, δ, V_c, and seafloor age for front-most volcanoes. Convergence velocities that include back-arc spreading rates are shown in light gray. Volcanoes with unconstrained ages are evenly distributed as being from the Cretaceous Quiet Period and are shown in light gray in Figure 8e.

and S2b) shows a large variety of H, H', slab dips, rates of convergence, and incoming seafloor ages. In these compilations, 99% of H estimates lie between 58 and 203 km and 50% between 85 and 119 km. Averaging H for 500-km sections of arc results in a range in H from 72 ± 9 km in the central Aleutians, to 173 ± 16 km in northern Vanuatu. Taking medians, rather than means, of individual parameters has little effect. Similarly, H' varies from 83 to 208 km with the same end-members, and is on average 20 km greater than H. Globally, H averages 105 km with a median of 100 km (Figure 8). Horizontal distances from volcano to trench range from 85–90 km in Scotia and Vanuatu to 470 km in Alaska, with the middle 50% of arc-trench distances between 180 km and 275 km. Slab dips (δ) range from 17° in the central and northern Andes to 77° in

northern Vanuatu, with the middle 50% between 43° and 56°. Rates of convergence, corrected for obliquity with respect to the strike of the slab (V_c), range from 1.4 km/Ma in parts of the highly oblique Banda Sea to 100 km/Ma in the New Britain arc, not including back-arc rates (auxiliary material Table S1b). The middle 50% of V_c lies between 53 km/Ma and 76 km/Ma. The highest V_c includes back-arc spreading in Tonga, where the plate convergence rate is 225 km/Ma [*Zellmer and Taylor*, 2001]. Overall, these values show a rate, geometry and duration of subduction-zone processes consistent with those assumed in many geodynamic models: the typical, median subduction zone has H = 100 km (H' = 121 km) with a slab dipping 50° and subducting seafloor 56 Ma old at 69 km/Ma.

[27] Where H could be calculated, incoming seafloor ages range from 15 Ma off Costa Rica to 155 Ma off the Marianas, with the middle 50% between 42 Ma and 107 Ma. Volcanoes with incoming plates younger than 15 Ma do not have H estimates because intermediate depth seismicity is largely absent. The distribution of incoming seafloor ages has two peaks, one at 50 Ma, and one around 100 Ma, both for individual volcanoes and for averages for 500-km sections of arc, in agreement with previous analyses [*Parsons*, 1982]. We see no discernable correlation (R = −0.27 for 48 arc segments) between convergence velocities and seafloor ages. Hence seafloor production and consumption rates have varied over the past 170 Ma.

4.2. Global Variations in H′

[28] We compare all tabulated subduction parameters, and various combinations of them, with H' for 500-km along-strike averages (Figure 9; Table 1; auxiliary material Table S1a and S1b). For each parameter pair, we calculate the linear correlation coefficient R and a confidence P, the probability that the observed correlation could arise by chance as estimated from the asymptotic normal approximation [*Press et al.*, 1986]. The correlations are generally weak, the only significant correlation at 95% confidence is between H' and δ (R = 0.54, P = 0.016%). For uncorrected H this correlation is weaker (R = 0.38, P = 0.98%) but still significant at 95% confidence. The sign of the correlation is opposite of that expected from the effects discussed in section 3.3, indicating that hypocentral errors do not create this correlation. Such a correlation has been hypothesized previously [*Davies and Stevenson*, 1992] as a consequence of fluids having to migrate through a boundary layer before reaching the mantle-melting region. If the boundary layer thickness does not vary with δ, then steeper slabs will result in greater apparent H. The same geometrical effect occurs for any process that displaces the melting region by a constant distance away from the WBZ (Figure 10). For this geometry the relevant independent variable should be $q = 1/\cos\delta$, and the correlations improve when q is used instead of δ (for H' or H versus q, R = 0.65 or 0.50 respectively).

[29] By comparison, *England et al.* [2004] found no correlation between H and δ but found a statistically significant negative correlation between H and the plate descent rate, $V_c\sin\delta$. They explain the correlation as a consequence of the way in which heat advects into the mantle wedge; faster subduction advects heat more rapidly toward the shallow part of the subduction system [*England and Wilkins*, 2004]. We do not observe this correlation (R = 0.09; P = 55%). The primary difference between our two analyses is the addition of several arcs to our data set including Vanuatu, the Solomons, New Britain, the Philippines, Nicaragua, and the eastern Sunda arc (Figure 1). Elimination of these arcs, 20% of the data set, would lead to correlations similar to theirs (Figure 9e); however, it is not clear that there is a basis for doing so. Most are places of known recent collisions, arc polarity reversals or arc migrations, so tectonic complexity may alter the H-descent rate relationship, but the same is true for many arcs examined in both studies. The added arcs also include most of those with high slab dip (δ > 60°), which explains why we observe a strong correlation between H and δ while *England et al.* [2004] do not. These steeply dipping slabs control the H-δ trend in our data.

[30] However, correlations do exist between H' and $V_c\sin\delta$ for large subsets of the data set, suggesting that the descent rate effect plays a role in localizing arc volcanoes. This is most obvious by considering the 8000 km of the global arc system that extends from Alaska through the Marianas (Figure 9). The Pacific plate subducts here with minimal tectonic complexity, while H' varies over most of its range. For this section, H' correlates strongly with descent rate (R = −0.85, P = 0.0058%; or R = −0.79, P = 0.037% if back-arc strain is considered). Thus the hypothesis of *England et al.* [2004] reasonably explains this major suite of subduction zones, for which δ is generally low to moderate. Hypocentral accuracies are relatively high in the northern Pacific, so perhaps improvements to the southern-hemisphere seismic monitoring will make such

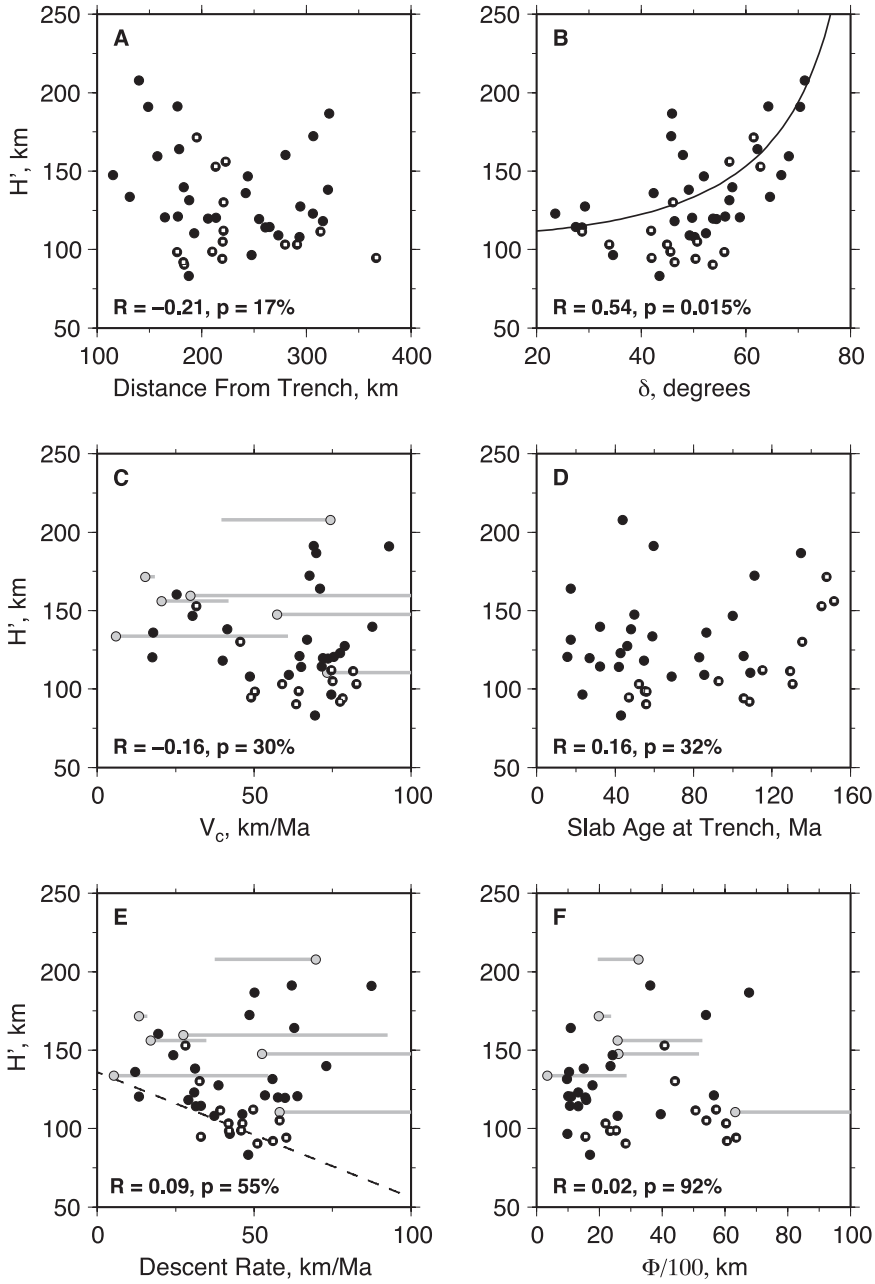

Figure 9. Distance from trench, average slab dip (δ), average downdip velocity (V_c), seafloor age, descent rate, and thermal parameter (Φ) versus H' for 500-km sections of arc. Values for sections with back-arc spreading or compression are shown as gray circles with lines to values including back-arc strains. Northern Pacific arcs (Alaska through the Marianas) are highlighted with white centers. The solid line in Figure 9b is the best fit line to 1/cos(δ). The dashed line in Figure 9e is the best fit line to data from *England et al.* [2004].

correlations more apparent globally in future analyses.

4.3. Variation in H Within Arc Segments

[31] It is reasonable to expect that mantle flow is complicated in many settings, that slab and volcano geometry are not in steady state, that three-dimensional flow effects perturb the melting regime near slab tears and ends, and that subduction of anomalously thick crust alters the magma generation process. The data show many examples of H varying systematically by tens of kilometers over short distances (<200 km) within arc segments, perhaps due to such effects. This section examines the largest such variations.

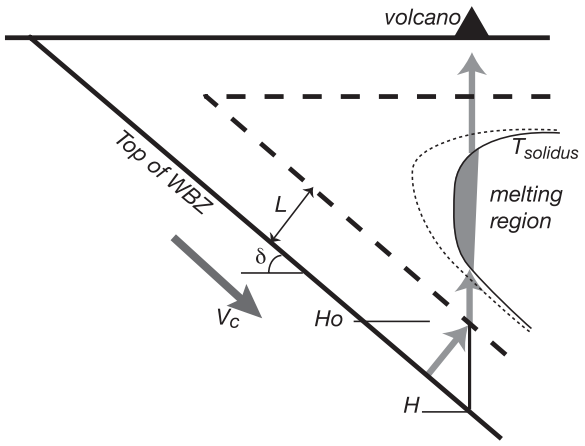

Figure 10. Schematic controls on *H*. Gray lines show simplified fluid and melt transport path from slab to arc. Thick dashed line demarks limit of wedge flow, displaced by *L* from WBZ; *L* represents thermal boundary layer and displacement of corrected WBZ from slab surface. Fluid enters the flowing part of wedge at depth *Ho*, shallower than observed *H* by $L/\cos\delta$; *Davies and Stevenson* [1992] predict similar effect. Within wedge, location of solidus (thin line) varies with slab descent rate $V_c\sin\delta$ [*England et al.*, 2004]; dashed line shows schematic effect of increasing descent rate. Thus *H* could correlate positively with $1/\cos\delta$ and negatively with $V_c\sin\delta$.

4.3.1. Java

[32] The largest along-strike variation takes place at the volcanic front in Java, where *H* shifts by 70 km on either side of 108°E longitude. *H* averages 90 km west of 108°E through southeastern Sumatra, and 150 km to the east, changing over a distance of <150 km along strike. This jump appears to be formed at the overlapping of the ends of two volcanic lines (Figure 11). Slab shape changes little across this boundary. Deep seismicity (>500 km depth) does vanish west of ~105°E [e.g., *Widiyantoro and van der Hilst*, 1996], which may indicate along-strike changes in mantle flow, but the WBZ shape above 250 km depth shows little along-strike variation. The dominant change is a shift in the location of the volcanoes in relation to slab and the trench. Roughly 1200 km eastward, east of 119°E (western Banda Sea), the volcanoes step back toward to the trench, and slab depths once again become near 100 km.

[33] It is not clear what causes this shift. The thermal parameter Φ increases from $4{\cdot}10^3$ km west of 105° to $5.6{\cdot}10^3$ km east of 105°, although similar changes occur between neighboring arc segments elsewhere for which there are no changes in *H*. Arc geochemistry also varies, and variations in potassium have been found previously to correlate with *H* and distance from the trench, part of the global "K-H" trend [*Hatherton and Dickinson*, 1969; *Whitford*, 1979]. *Wheller et al.* [1987] found a sharp increase in K_{Si}, a parameter based on the ratio of potassium to silica, to follow the increase in *H* at 108°E longitude, and a subsequent decrease in both K_{Si} and *H* in the western Banda Sea. Thus the Java volcanoes exhibit some geochemical variations that may reflect changes in *H* due to shift in arc position, but the cause for the arc step is not obvious.

4.3.2. Central America

[34] Similar shifts in volcano location relative to the trench and slab appear to be the dominant cause of changes in *H* within Central America. Two

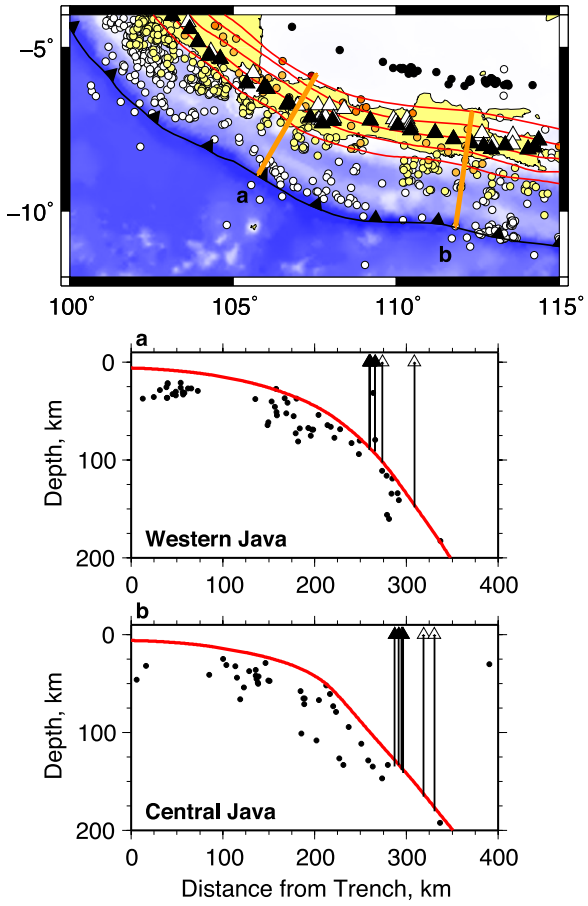

Figure 11. Cross sections of EHB seismicity beneath Java, showing estimates of *H*. Earthquakes and volcanoes in map view follow the color scheme of Figure 1. Earthquakes are projected onto the cross sections with a 100-km half width, and volcanoes are projected with a 75-km half width. Black triangles are front-most volcanoes; white triangles are other volcanoes. Note change in volcano locations.

changes in-depth occur at −86.3° and −85.5° longitude, at steps in the volcanic front that correlate with geochemical variations [*Carr et al.*, 2003]. The largest of these jumps is at −85.5° where H changes from 130–140 km in Nicaragua to 80–100 km in Costa Rica within 50 km along strike, as the arc steps roughly 40 km toward the trench (Figures 2d and 2e and auxiliary material Figure S2). This discontinuity has been previously observed [e.g., *Carr and Stoiber*, 1977; *Protti et al.*, 1994], with no evidence for a slab contortion. It may correspond to changes in the structure and perhaps composition of the upper plate [*Carr et al.*, 2003], corresponding to a terrane boundary between continental crust in Nicaragua and an oceanic plateau in Costa Rica. The Nicaragua segment shows 50 km trenchward migration in the last 10 Ma [*Plank et al.*, 2002], so the slab and arc geometry may be out of equilibrium. Of course, transient geometries may be present elsewhere, but this is one of the few places where rapid recent arc migration is well documented.

4.3.3. Central Andes

[35] In the central Andes, between −21° and −24° latitude, H increases from 100 km to 130 km, near 23°S, across a total distance of 300 km (Figure 12). *Schurr and Rietbrock* [2004] have interpreted attenuation measurements to indicate the existence of a cool, strong fore-arc mass extending to ~110 km depth. This may impede magma generation, causing a shift in the volcanic front and increasing H. Thus heterogeneity of the mantle wedge might affect arc location.

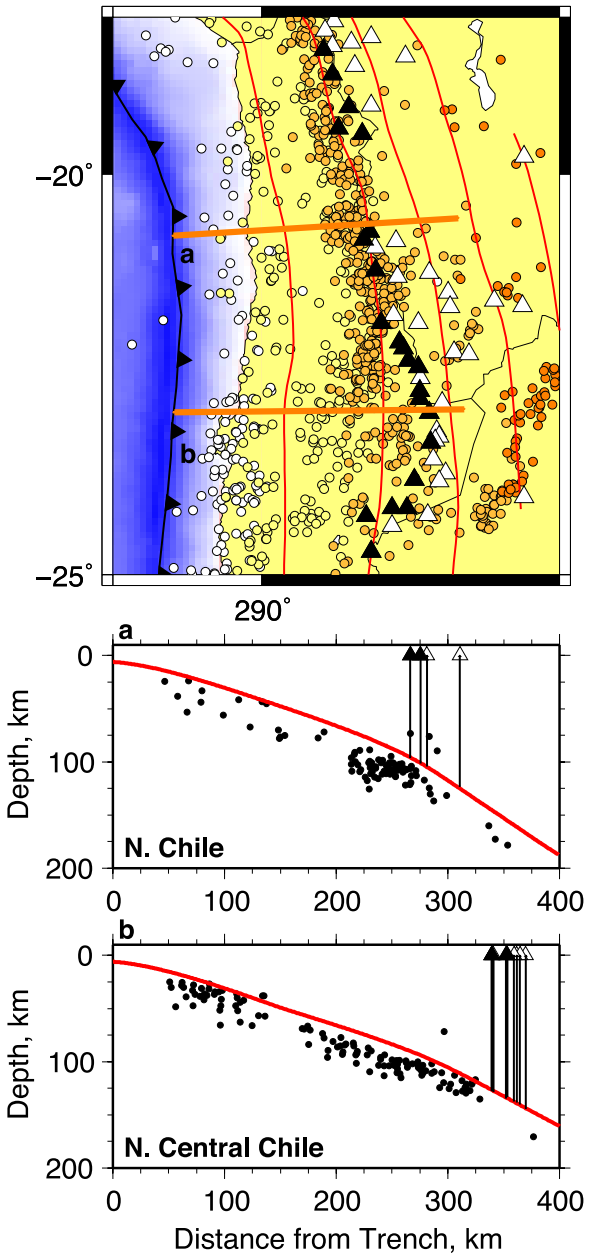

Figure 12. Cross sections of EHB seismicity beneath the northern Andes, exhibiting the increase in H behind the Atacama block, with little change in the slab surface. Earthquakes and volcanoes in map view follow the color scheme of Figure 1 and are projected with a 50-km half width.

4.4. Apparent WBZ Thickness and Double Seismic Zones

[36] The measurement of slab width used to estimate scatter in hypocenters also provides some insight into internal structure of the WBZ. In Northern Honshu, cross sections (Figure 2a) suggest a double seismic zone in agreement with other studies [*Yoshii*, 1979; *Igarashi et al.*, 2001]. This area has the smallest formal earthquake location errors e_f of any arc segment, and it also has a broad apparent WBZ thickness, showing two peaks in the distribution of earthquakes relative to the WBZ surface (Figure 5a). For the Kuriles and Tonga, where double seismic zones have been suggested previously [*Kao and Chen*, 1994; *Kawakatsu*, 1985], we only find weak evidence for bimodal distributions of earthquakes perpendicular to WBZ surfaces, probably because the hypocentral errors are relatively large and comparable to the seismic zone widths (Figures 5b and 5c).

[37] As discussed in section 3.3, the apparent thickness of the seismic zone exceeds that predicted from formal errors by up to 45 km. A significant positive correlation exists ($R = 0.54$, $P =$

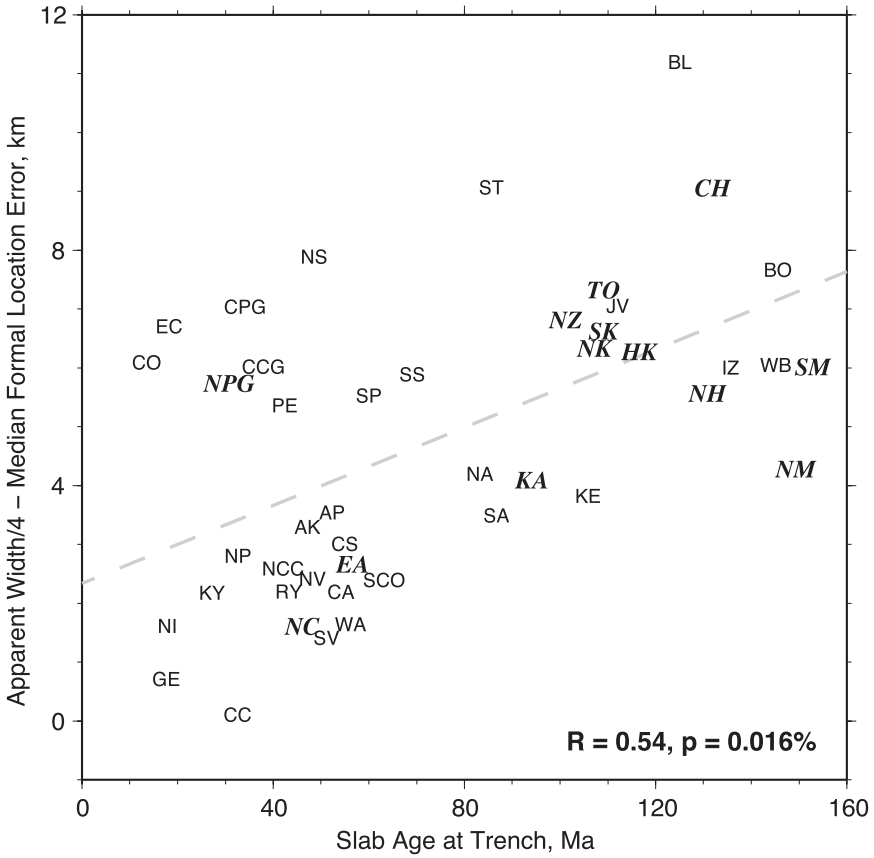

Figure 13. Comparison of the difference between the standard deviation of earthquake-slab distance and the average formal errors in earthquake locations, to the average age of the incoming seafloor at the trench for 500-km sections of arc containing more than 10 earthquakes from the EHB catalog. Note that most double seismic zones have incoming seafloor ages greater than 80 Ma and that volcanic gaps underlain by flat subduction (represented by CPG, CCG, and NPG) have thick seismic zones, particularly in comparison to other arc sections with similar incoming seafloor ages. Abbreviations for arc section names are listed in auxiliary material Table S1. Italicized and boldface abbreviations represent slabs that have been suggested in other studies to contain double seismic zones. Peru: *Isacks and Barazangi* [1977], Northern Chile: *Comte et al.* [1999], Alaska: *Ratchoversusky et al.* [1997], Eastern Aleutians: *Reyners and Coles* [1982]; *Abers* [1992], Kamchatka and Kuriles: *Kao and Chen* [1994], Hokkaido: *Suzuki and Motoya* [1981], Honshu: e.g., *Hasegawa et al.* [1978], Marianas: *Samowitz and Forsyth* [1981], New Britain (not pictured): *McGuire and Wiens* [1995], Tonga: *Kawakatsu* [1985], New Zealand: *Robinson et al.* [1997].

0.016%) between excess WBZ thickness (observed thickness – $4e_f$) and incoming plate age (Figure 13). Such a correlation implies that older plates have thicker WBZs, as expected since older plates will have a thicker region of low temperatures and hence thicker regions in which earthquakes could occur [e.g., *Hacker et al.*, 2003]. Many of these may be sites of double seismic zones, such as in Honshu, and most well-documented double zones correspond to arc segments where the WBZ is wide compared with formal errors (Figure 13). On the basis of this logic, several other arc segments also emerge as wide potential double seismic zones at intermediate depths, including several parts of the Sunda arc, Izu, and Bonin. In any case, the correlation between apparent WBZ width and incoming plate age emphasizes the important role of thermal structure in controlling seismicity.

4.5. Geochemical Trends

[38] The volcano-specific estimates of H and other parameters provide insight into systematic variations seen in arc geochemistry [e.g., *Plank and Langmuir*, 1988, 1998; *Stern*, 2002]. We present one example here to illustrate how H might be an important factor in such analyses. Figure 14 shows that H for individual volcanoes along Central

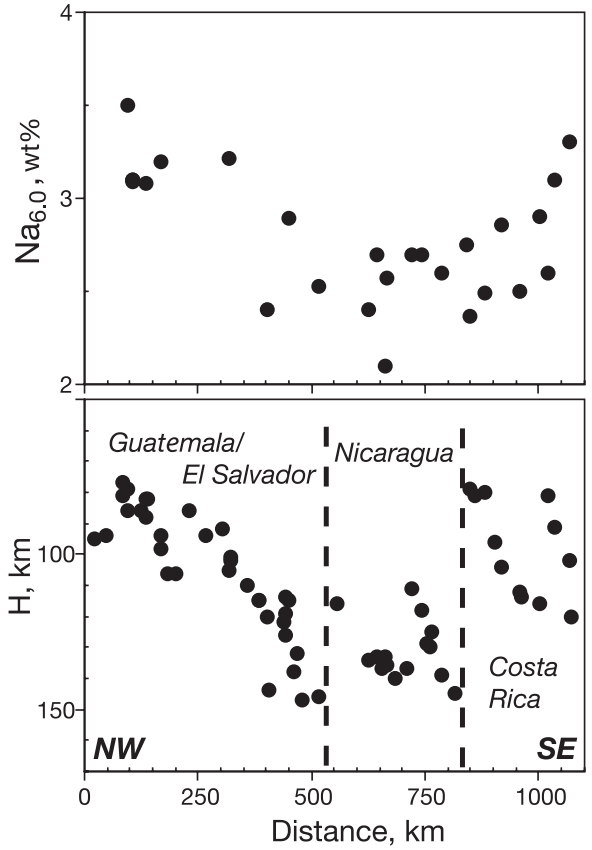

Figure 14. Geochemical systematics along strike in Central America, compared with *H*. $Na_{6.0}$ is Na_2O concentration of each volcanic magma series at 6 wt% MgO, determined from Na_2O-MgO linear regression, as in *Plank and Langmuir* [1988]. Volcanic data from Centam database of *Carr and Rose* [1987]. Greater *H* leads to greater extent of melting and lower $Na_{6.0}$.

America varies along strike with Na in arc lavas. Here, Na is derived from the Centam database [*Carr and Rose*, 1987], screened and converted to $Na_{6.0}$ following *Plank and Langmuir* [1988]. Na is incompatible during melting so is abundant in low-degree melts, becoming dilute as the degree of mantle melting increases. The degree of melting should be limited by the vertical size of the region available for melting, as evident in global correlations between upper-plate crustal thickness and $Na_{6.0}$ [*Plank and Langmuir*, 1988]. The correlation between $Na_{6.0}$ and *H* (Figure 14) also can be explained as an effect of the melting region size; larger *H* increases the vertical size of the mantle wedge beneath the arc, leading to higher degrees of melting and lower $Na_{6.0}$. Of course, other variables also change along strike, but the covariation observed here suggests that changes in *H* may be a major factor in determining the extent of melting.

5. Conclusions

[39] A global compilation of subduction parameters is presented, including a volcano-specific compilation of WBZ depth *H* beneath arc volcanoes (auxiliary material). The compilation allows the relationship between subduction parameters to be reassessed, with three primary results.

[40] 1. The depth of subducting plates beneath volcanic arcs, *H*, varies systematically both between arc segments globally and within them by a factor of 2–3. This variation exceeds the uncertainties in *H* by several times, particularly once hypocentral errors are corrected for (*H*'). Thus the volcanic front is controlled by factors other than slab depth, a point made by previous authors. In some regions, *H* varies by several tens of km within along-strike distances of 150 km, suggesting that secondary processes such as temporal changes in slab dip or heterogeneities in wedge structure can have a dominant effect. Globally, slab dip δ correlates with *H*, possibly a boundary layer effect.

[41] 2. The digitized slab surfaces also provide a reference to investigate global variations in WBZ internal structure. In all slab segments, WBZ seismicity appears thicker than expected from error analysis, perhaps reflecting actual thickness of the seismic zone such as caused by double seismic zones in some segments. This extra thickness increases with increasing plate age, as expected if WBZ seismicity is limited by temperature.

[42] 3. Geochemical proxies for the melting process correlate with *H*, in at least one instance. This is not surprising, as the size of the melting regime is fundamentally controlled by the slab geometry relative to the volcanic arc. It is expected that many more examples of *H* affecting arc melting will be found.

Acknowledgments

[43] This project benefited from feedback at a MARGINS Theoretical workshop, extensive comments and a figure from T. Plank, and thoughtful, constructive reviews from R. Van der Hilst, D. Wiens, and editor P. Van Keken. L. Auger and G. Rossi contoured seismicity for repeatability tests, and N. Harmon contributed extensively to the slab digitization effort. P. England graciously provided preprints of his papers in the course of this effort, and Bob Engdahl made the EHB catalog updates available as they came out. Many figures are

made using GMT [*Wessel and Smith*, 1991]. This effort partly supported by NSF grant EAR0215577.

References

Abers, G. A. (1992), Relationship between shallow-depth and intermediate-depth seismicity in the eastern Aleutian subduction zone, *Geophys. Res. Lett.*, *19*(20), 2019–2022.

Arculus, R. J. (2003), Cruise Summary, Tonga-Eastern Lau Vents Expedition, report, Australia Natl. Univ., Canberra.

Arculus, R. J. (2004), Cruise Summary, Northern Tonga Vents Expedition, report, Australia Natl. Univ., Canberra.

Bowin, C., G. M. Purdy, C. Johnston, G. Shor, L. Lawver, H. M. S. Hartono, and P. Jezek (1980), Arc-continent collision in Banda Sea region, *AAPG Bull.*, *64*(6), 868–915.

Carr, M. J., and W. I. Rose, Jr. (1987), CENTAM: A database of Central American volcanic rocks, *J. Volcanol. Geotherm. Res.*, *33*(1–3), 239–240.

Carr, M. J., and R. E. Stoiber (1977), Geologic setting of some destructive earthquakes in Central America, *Geol. Soc. Am. Bull.*, *88*(1), 151–156.

Carr, M. J., M. D. Feigenson, L. C. Patino, and J. A. Walker (2003), Volcanism and geochemistry in Central America: Progress and problems, in *Inside the Subduction Factory*, *Geophys. Monogr. Ser.*, vol. 138, edited by J. Eiler, pp. 153–179, AGU, Washington, D. C.

Comte, D., L. Dorbath, M. Pardo, T. Monfret, H. Haessler, L. Rivera, M. Frogneux, B. Glass, and C. Meneses (1999), A double-layered seismic zone in Arica, northern Chile, *Geophys. Res. Lett.*, *26*(13), 1965–1968.

Davies, J. H., and D. J. Stevenson (1992), Physical model of source region of subduction zone volcanics, *J. Geophys. Res.*, *97*(B2), 2037–2070.

DeMets, C., R. G. Gordon, D. F. Argus, and S. Stein (1994), Effect of recent revisions to the geomagnetic reversal timescale on estimates of current plate motions, *Geophys. Res. Lett.*, *21*(20), 2191–2194.

Engdahl, E. R., R. van der Hilst, and R. Buland (1998), Global teleseismic earthquake relocation with improved travel times and procedures for depth determination, *Bull. Seismol. Soc. Am.*, *88*(3), 722–743.

England, P., and C. Wilkins (2004), A simple analytical approximation to the temperature structure in subduction zones, *Geophys. J. Int.*, *159*(3), 1138–1154.

England, P., R. Engdahl, and W. Thatcher (2004), Systematic variation in the depths of slabs beneath arc volcanoes, *Geophys. J. Int.*, *156*(2), 377–408.

Ferris, A., G. A. Abers, D. H. Christensen, and E. Veenstra (2003), High resolution image of the subducted Pacific (?) Plate beneath central Alaska, 50–150 km depth, *Earth Planet. Sci. Lett.*, *214*(3–4), 575–588.

Gill, J. (1981), *Orogenic Andesites and Plate Tectonics*, Springer, New York.

Gorbatov, A., and V. Kostoglodov (1997), Maximum depth of seismicity and thermal parameter of the subducting slab: General empirical relation and its application, *Tectonophysics*, *277*, 165–187.

Gudmundsson, O., and M. Sambridge (1998), A regionalized upper mantle (RUM) seismic model, *J. Geophys. Res.*, *103*(B4), 7121–7136.

Hacker, B. R., S. M. Peacock, G. A. Abers, and S. D. Holloway (2003), Subduction factory: 2. Are intermediate-depth earthquakes in subducting slabs linked to metamorphic dehydration reactions?, *J. Geophys. Res.*, *108*(B1), 2030, doi:10.1029/2001JB001129.

Hasegawa, A., N. Umino, and A. Takagi (1978), Double-planed structure of the deep seismic zone in the northeastern Japan Arc, *Tectonophysics*, *47*(1–2), 43–58.

Hatherton, T., and W. R. Dickinson (1969), The relationship between andesitic volcanism and seismicity in Indonesia, the Lesser Antilles, and other island arcs, *J. Geophys. Res.*, *74*(22), 5301–5310.

Igarashi, T., T. Matsuzawa, N. Umino, and A. Hasegawa (2001), Spatial distribution of focal mechanisms for interplate and intraplate earthquakes associated with the subducting Pacific plate beneath the northeastern Japan arc: A triple-planed deep seismic zone, *J. Geophys. Res.*, *106*(B2), 2177–2192.

Isacks, B. L., and M. Barazangi (1977), Geometry of Benioff zones: Lateral segmentation and downwards bending of the subducted lithosphere, in *Island Arcs, Deep Sea Trenches and Back Arc Basins*, *Maurice Ewing Ser.*, *1*, edited by M. Talwani and W. C. Pitman III, pp. 99–114, AGU, Washington D. C.

Kao, H., and W.-P. Chen (1994), The double seismic zone in Kuril-Kamchatka: The tale of two overlapping single zones, *J. Geophys. Res.*, *99*(B4), 6913–6930.

Kato, T., J. Beavan, T. Matsushima, Y. Kotake, J. T. Camacho, and S. Nakao (2003), Geodetic evidence of back-arc spreading in the Mariana Trough, *Geophys. Res. Lett.*, *30*(12), 1625, doi:10.1029/2002GL016757.

Kawakatsu, H. (1985), Double seismic zone in Tonga, *Nature*, *316*(6023), 53–55.

Kerrick, D. M., and J. A. D. Connolly (2001), Metamorphic devolatilization of subducted oceanic metabasalts: Implications for seismicity, arc magmatism and volatile recycling, *Earth Planet. Sci. Lett.*, *189*(1–2), 19–29.

Kirby, S. H., E. R. Engdahl, and R. P. Denlinger (1996), Intermediate-depth intraslab earthquakes and arc volcanism as physical expressions of crustal and uppermost mantle metamorphism in subducting slabs, in *Subduction Top to Bottom*, *Geophys. Monogr. Ser.*, vol. 96, edited by G. E. Bebout et al., pp. 195–214, AGU, Washington, D. C.

Kisslinger, C. (1993), Seismicity in subduction zones from local and regional network observations, *Pure Appl. Geophys.*, *140*(2), 257–285.

McGuire, J. J., and D. A. Wiens (1995), A double seismic zone in New-Britain and the morphology of the Solomon plate at intermediate depths, *Geophys. Res. Lett.*, *22*(15), 1965–1968.

McLaren, J. P., and C. Frohlich (1985), Model calculations of regional network locations for earthquakes in subduction zones, *Bull. Seismol. Soc. Am.*, *75*(2), 397–413.

Müller, R. D., W. R. Roest, J.-Y. Royer, L. M. Gahagan, and J. G. Sclater (1997), Digital isochrons of the world oceans, *J. Geophys. Res.*, *102*(B2), 3211–3214.

Nakajima, J., T. Matsuzawa, A. Hasegawa, and D. Zhao (2001), Three-dimensional structure of V_p, V_s, and V_p/V_s beneath northeastern Japan: Implications for arc magmatism and fluids, *J. Geophys. Res.*, *106*(B10), 21,843–21,858.

Parsons, B. (1982), Causes and consequences of the relation between area and age of the ocean floor, *J. Geophys. Res.*, *87*(B1), 289–302.

Pavlis, G. L. (1986), Appraising earthquake hypocenter location errors: A complete, practical approach for single-event locations, *Bull. Seismol. Soc. Am.*, *76*, 1699–1717.

Plank, T., and C. H. Langmuir (1988), An evaluation of the global variations in the major element chemistry of arc basalts, *Earth Planet. Sci. Lett.*, *90*(4), 349–370.

Plank, T., and C. H. Langmuir (1998), The chemical composition of subducting sediment and its consequences for the crust and mantle, *Chem. Geol.*, *145*(3–4), 325–394.

Plank, T., V. Balzer, and M. Carr (2002), Nicaraguan volcanoes record paleoceanographic changes accompanying closure of the Panama gateway, *Geology*, *30*(12), 1087–1090.

Press, W. H., S. A. Teukolsky, W. T. Vetterling, and B. P. Flannery (1986), *Numerical Recipes in C: The Art of Scientific Computing*, Cambridge Univ. Press, New York.

Protti, M., F. Gundel, and K. McNally (1994), The geometry of the Wadati-Benioff zone under southern Central-America and its tectonic significance: Results from a high-resolution local seismographic network, *Phys. Earth Planet. Inter.*, *84*(1–4), 271–287.

Ratchkovsky, N. A., J. Pujol, and N. N. Biswas (1997), Relocation of earthquakes in the Cook Inlet area, South Central Alaska, using the joint hypocenter determination method, *Bull. Seismol. Soc. Am.*, *87*(3), 620–636.

Reyners, M., and K. S. Coles (1982), Fine structure of the dipping seismic zone and subduction mechanics in the Shumagin Islands, Alaska, *J. Geophys. Res.*, *87*(1), 356–366.

Robinson, R., R. Benites, and R. J. Van Dissen (1997), Evidence for temporal clustering of large earthquakes in the Wellington region from computer models of seismicity, paper presented at New Zealand National Society for Earthquake Engineering Technical Conference, Wairakei, New Zealand.

Samowitz, I. R., and D. W. Forsyth (1981), Double seismic zone beneath the Mariana island arc, *J. Geophys. Res.*, *86*(B8), 7013–7021.

Schmidt, M. W., and S. Poli (1998), Experimentally based water budgets for dehydrating slabs and consequences for arc magma generation, *Earth Planet. Sci. Lett.*, *163*(1–4), 361–379.

Schurr, B., and A. Rietbrock (2004), Deep seismic structure of the Atacama basin, northern Chile, *Geophys. Res. Lett.*, *31*, L12601, doi:10.1029/2004GL019796.

Sella, G. F., T. H. Dixon, and A. Mao (2002), REVEL: A model for recent plate velocities from space geodesy, *J. Geophys. Res.*, *107*(B4), 2081, doi:10.1029/2000JB000033.

Siebert, L., and T. Simkin (2002), Volcanoes of the world: An illustrated catalog of Holocene volcanoes and their eruptions, *Global Volcanism Program Digital Inf. Ser., GVP-3*, Smithsonian Inst., Washington, D. C. (Available at http://www.volcano.si.edu/world/)

Stern, R. J. (2002), Subduction zones, *Rev. Geophys.*, *40*(4), 1012, doi:10.1029/2001RG000108.

Strauch, W., et al. (2004), Sismos y volcanes de Nicaragua, report, Inst. Nicaragüense de Estud. Territ., Managua.

Suzuki, S., and Y. Motoya (1981), Double seismic zone under Hokkaido, in *Report of the Coordinating Committee for Earthquake Prediction*, vol. 25, p. 8, Tokyo.

Tatsumi, Y. (1986), Formation of the volcanic front in subduction zones, *Geophys. Res. Lett.*, *13*(8), 717–720.

Tatsumi, W., and S. Eggins (1995), *Subduction Zone Magmatism*, Blackwell Sci., Malden, Mass.

Taylor, F. W., et al. (1995), Geodetic measurements of convergence at the New-Hebrides-Island Arc indicate arc fragmentation caused by an impinging aseismic ridge, *Geology*, *23*(11), 1011–1014.

Thomas, C., R. Livermore, and F. Pollitz (2003), Motion of the Scotia Sea plates, *Geophys. J. Int.*, *155*(3), 789–804.

Tichelaar, B. W., and L. J. Ruff (1993), Depth of seismic coupling along subduction zones, *J. Geophys. Res.*, *98*(B2), 2017–2037.

Tsuboi, S. (1992), Japan Univ. network earthquake catalog, *Eos Trans. AGU*, *73*(43), Fall Meet. Suppl., 344.

van der Hilst, R. D., and E. R. Engdahl (1992), Step-wise relocation of ISC earthquake hypocenters for linearized tomographic imaging of slab structure, *Phys. Earth Planet. Inter.*, *75*(1–3), 39–53.

Wallace, L. M., C. Stevens, E. Silver, R. McCaffrey, W. Loratung, S. Hasiata, R. Stanaway, R. Curley, R. Rosa, and J. Taugaloidi (2004), GPS and seismological constraints on active tectonics and arc-continent collision in Papua New Guinea: Implications for mechanics of microplate rotations in a plate boundary zone, *J. Geophys. Res.*, *109*, B05404, doi:10.1029/2003JB002481.

Wessel, P., and W. H. F. Smith (1991), Free software helps map and display data, *Eos Trans. AGU*, *72*(41), 445–446, 441.

Wheller, G. E., R. Varne, J. D. Foden, and M. J. Abbott (1987), Geochemistry of Quaternary volcanism is the Sunda-Banda arc, Indonesia, and 3-component genesis of island-arc basaltic magmas, *J. Volcanol. Geotherm. Res.*, *32*(1–3), 137–160.

Whitford, J. D. (1979), Spatial variations in the geochemistry of Quaternary lavas across the Sunda arc in Java and Bali, *Contrib. Mineral. Petrol.*, *70*, 341–356.

Widiyantoro, S., and R. van der Hilst (1996), Structure and evolution of lithospheric slab beneath the Sunda arc, Indonesia, *Science*, *271*, 1566–1570.

Yoshii, T. (1979), A detailed cross-section of the deep seismic zone beneath northeastern Honshu, Japan, *Tectonophysics*, *55*(3–4), 349–360.

Yuan, X., et al. (2000), Subduction and collision processes in the Central Andes constrained by converted seismic phases, *Nature*, *408*(6815), 958–961.

Zellmer, K. E., and B. Taylor (2001), A three-plate kinematic model for Lau Basin opening, *Geochem. Geophys. Geosyst.*, *2*(5), doi:10.1029/2000GC000106.

Zhao, D., T. Matsuzawa, and A. Hasegawa (1997), Morphology of the subducting slab boundary in the northeastern Japan arc, *Phys. Earth Planet. Inter.*, *102*, 89–104.